Breakdown of Magnetic Order in the Pressurized Kitaev Iridate β-Li_2IrO_3

M. Majumder,[1,*] R. S. Manna,[1,2,*] G. Simutis,[3] J. C. Orain,[3] T. Dey,[1] F. Freund,[1] A. Jesche,[1] R. Khasanov,[3] P. K. Biswas,[4] E. Bykova,[5] N. Dubrovinskaia,[5] L. S. Dubrovinsky,[6] R. Yadav,[7] L. Hozoi,[7] S. Nishimoto,[7] A. A. Tsirlin,[1,†] and P. Gegenwart[1]

[1]*Experimental Physics VI, Center for Electronic Correlations and Magnetism, University of Augsburg, 86159 Augsburg, Germany*

[2]*Department of Physics, IIT Tirupati, Tirupati 517506, India*

[3]*Laboratory for Muon Spin Spectroscopy, Paul Scherrer Institut, 5232 Villigen PSI, Switzerland*

[4]*ISIS Pulsed Neutron and Muon Source, STFC Rutherford Appleton Laboratory, Harwell Campus, Didcot, Oxfordshire OX11 0QX, United Kingdom*

[5]*Laboratory of Crystallography, Material Physics and Technology at Extreme Conditions, Universität Bayreuth, 95440 Bayreuth, Germany*

[6]*Bayerisches Geoinstitut, Universität Bayreuth, 95440 Bayreuth, Germany*

[7]*Institute for Theoretical Physics, IFW Dresden, 01069 Dresden, Germany*

(Received 19 February 2018; published 8 June 2018)

Temperature-pressure phase diagram of the Kitaev hyperhoneycomb iridate β-Li_2IrO_3 is explored using magnetization, thermal expansion, magnetostriction, and muon spin rotation measurements, as well as single-crystal x-ray diffraction under pressure and *ab initio* calculations. The Néel temperature of β-Li_2IrO_3 increases with the slope of 0.9 K/GPa upon initial compression, but the reduction in the polarization field H_c reflects a growing instability of the incommensurate order. At 1.4 GPa, the ordered state breaks down upon a first-order transition, giving way to a new ground state marked by the coexistence of dynamically correlated and frozen spins. This partial freezing in the absence of any conspicuous structural defects may indicate the classical nature of the resulting pressure-induced spin liquid, an observation paralleled to the increase in the nearest-neighbor off-diagonal exchange Γ under pressure.

DOI: 10.1103/PhysRevLett.120.237202

Introduction.—Quantum spin liquid is an exotic state of matter that entails highly correlated spins but evades magnetic ordering down to zero temperature [1]. The Kitaev model plays a special role in this context, because it offers an analytical solution for a quantum spin liquid and hosts fractionalized excitations having potential relevance to topological quantum computing [2–5]. The Kitaev spin liquid on the honeycomb lattice can be gapless or gapped, depending on the interaction regime. It shows peculiarities in the dynamical structure factor [6] and Raman response [7]. Many of these features are shared by the three-dimensional (3D) version of the Kitaev model on the hyperhoneycomb and stripyhoneycomb lattices [8–10]. One additional peculiarity in this case is that the spin-liquid phase survives to finite temperatures and undergoes a phase transition to a classical paramagnet [11,12]. This distinguishes the Kitaev spin liquid in 3D from any other instance of quantum spin liquid, because only the former shows a thermodynamic singularity [13].

On the experimental side, Kitaev physics in 3D can be relevant to β- and γ-polymorphs of Li_2IrO_3 [4]. Both compounds are magnetically ordered at low temperatures [14–17]. Their noncoplanar incommensurate spin arrangements are driven by the Kitaev interactions [18] in combination with other exchange terms producing the nearest-neighbor spin Hamiltonian [19–21]

$$H = \sum_{\langle ij\rangle;\alpha,\beta\neq\gamma} [J_{ij}\mathbf{S}_i\mathbf{S}_j + K_{ij}S_i^\gamma S_j^\gamma \pm \Gamma_{ij}(S_i^\alpha S_j^\beta + S_i^\beta S_j^\alpha)].$$

Here, J_{ij} is the Heisenberg exchange term, K_{ij} is the Kitaev exchange, and Γ_{ij} stands for the off-diagonal exchange anisotropy. These exchange parameters take different values for the X-, Y- and Z-type Ir-Ir bonds of the hyperhoneycomb lattice, respectively.

Long-range magnetic order in β- and γ-Li_2IrO_3 restricts access to the physics of the Kitaev model in 3D. *Ab initio* studies suggest that at least in β-Li_2IrO_3 magnetic interactions may change significantly under pressure [22], which should shift the system toward the exotic spin-liquid state. Experimental information remains limited to date, indicating only a reconstruction of the electronic state of Ir^{4+} below 2 GPa [23]. Here, we map out the temperature-pressure phase diagram of β-Li_2IrO_3 and show that the magnetic order disappears abruptly upon a first-order transition around 1.4 GPa, whereas local moments persist above this pressure and form a dynamic state, albeit hindered by partial spin freezing. We identify this state

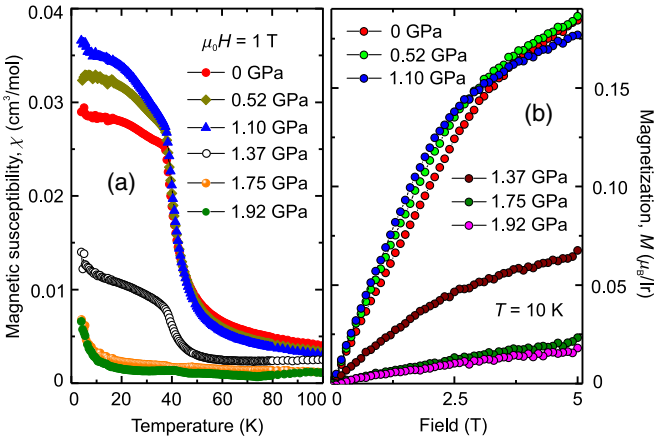

FIG. 1. (a) Magnetic susceptibility ($\chi = M/H$) as a function of temperature at different pressures in the presence of the 1 T magnetic field. (b) Magnetization curves measured at different pressures at 10 K.

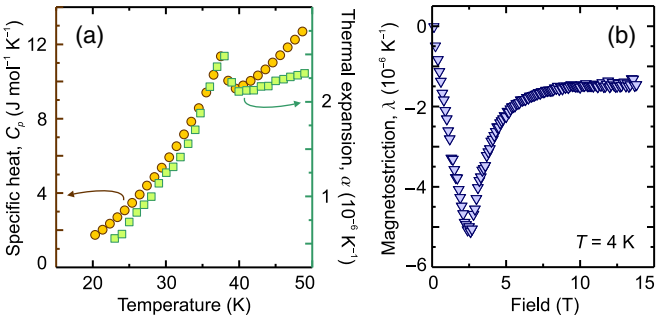

FIG. 2. (a) Specific heat and thermal expansion as function of temperature. (b) Magnetostriction at 4 K.

as a putative classical spin liquid in line with recent theory [24] suggesting the formation of such a correlated regime in the limit of large Γ, a trend consistent with the experimental evolution of the crystal structure and ensuing exchange couplings, which we obtain on different levels of *ab initio* theory.

Magnetization.—Magnetic susceptibility was measured on polycrystalline samples of β-Li_2IrO_3. It sharply increases below 50 K and changes slope at $T_N = 38$ K at ambient pressure [Fig. 1(a)]. This unusual behavior reflects the nontrivial incommensurate nature of the magnetic order [14], which is very sensitive to the applied field. The bend around $H_c \simeq 2.7$ T in the ambient-pressure magnetization curve [Fig. 1(b)] marks the suppression of the incommensurate order by the field applied along the b direction. Above 2.7 T, commensurate spin correlations reminiscent of the zigzag order become predominant [25]. The field couples to a ferromagnetic canting mode [21,25], and the value of the critical field H_c gauges the stability of the incommensurate order [26].

The same features are seen in the magnetization data under pressure measured upon compression. Below 1.1 GPa, T_N increases with the slope of $dT_N/dp \simeq 0.9$ K/GPa. The low-temperature susceptibility increases as well, reflecting the fact that the slope of $M(H)$ increases, and H_c shifts toward lower fields. Both features are suppressed at higher pressures and are no longer visible in the data collected at 1.7–1.9 GPa, where the signal becomes very low, reaching the sensitivity limit of our measurement setup. This suppression of the magnetization is well in line with the disappearance of the x-ray magnetic circular dichroism (XMCD) signal around 1.5 GPa [23], because XMCD is proportional to the sample magnetization induced by the applied field.

Thermal expansion and magnetostriction.—Evolution of the magnetic order under pressure was cross-checked by ambient-pressure thermal expansion measurements performed on the pressed pellet of β-Li_2IrO_3. Figure 2(a) shows a λ-like peak in the thermal expansion (α), indicating a second-order phase transition with a non-negligible magnetoelastic coupling. The initial slope of T_N is obtained from the Ehrenfest relation $dT_N/dp = V_{\mathrm{mol}} \times T_N \times \Delta\beta/\Delta C$. In our case, $V_{\mathrm{mol}} = 3.354 \times 10^{-5}$ m^3/mol and volume expansion coefficient $\beta = 3\alpha$, with $\Delta\alpha = -(0.5 \pm 0.05) \times 10^{-6}$ K^{-1}, yields an initial pressure dependence of the transition temperature $(dT_N/dp)_{p\to 0} = (0.7 \pm 0.02)$ K/GPa in agreement with the magnetization data. This confirms the positive sign of dT_N/dp.

Figure 2(b) shows the magnetostriction coefficient $\lambda = d[\Delta L(T)/L_0]/dB$ [27,28] at 4 K as a function of the magnetic field. The hump around 2.7 T develops below T_N, indicating magnetoelastic coupling in the ordered state. The negative sign of λ implies that the magnetization should increase upon compression, following the Maxwell relation $\lambda V = -(dM/dp)_{T,B}$, where V is the volume and M is the magnetization. This further supports the increase in M and the reduction in H_c under pressure.

The field H_c marks an instability of the incommensurate state [25,26]. The reduction in H_c upon compression implies that the ambient-pressure magnetic order becomes destabilized and should eventually disappear, as we observe indeed. However, neither the magnetization data nor XMCD elucidate the nature of the high-pressure phase formed above 1.4 GPa. The low magnetization and the absent XMCD signal could imply (i) a robust antiferromagnetic order that is not polarized by the field of several Tesla, as in α-Li_2IrO_3 and Na_2IrO_3, (ii) a dynamic spin state, and (iii) magnetism collapse due to, e.g., dimerization [29] or metallization. In the following, we use muon spin relaxation (μSR) as a sensitive local probe that distinguishes between these different scenarios and gives strong evidence for the formation of a dynamic spin state, albeit hindered by partial spin freezing.

μSR results.—Muon spin relaxation experiments were performed on polycrystalline samples. We discuss the ambient-pressure data first. At temperatures below T_N, μSR spectra exhibit well-defined oscillations, which indicate long-range magnetic order. Given the complex

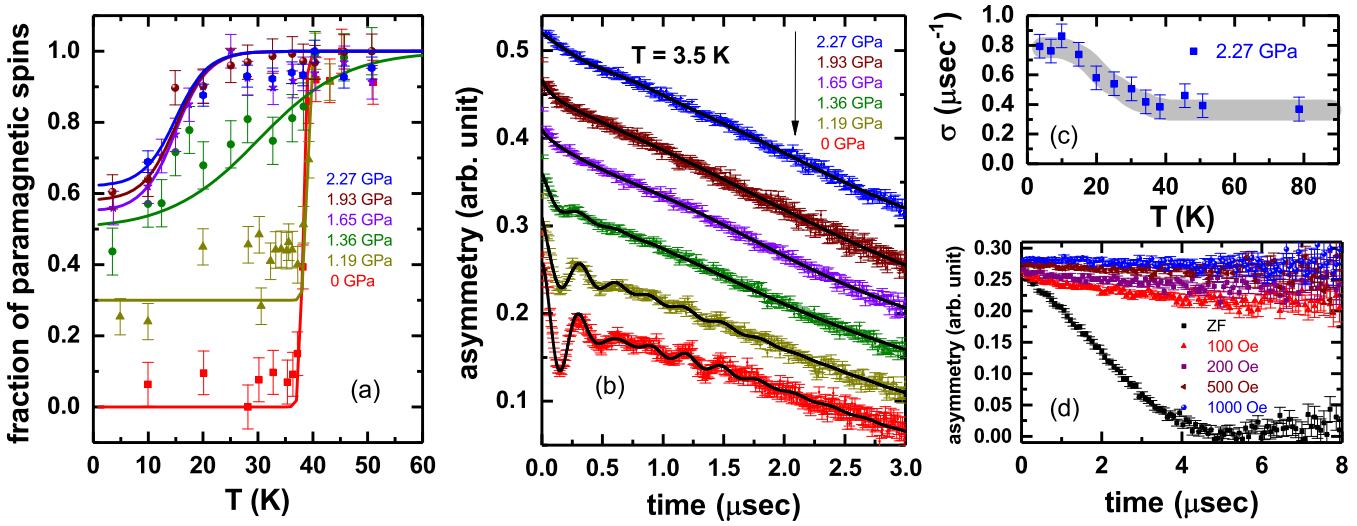

FIG. 3. (a) Volume fraction of dynamic spins measured in the WTF experiment; the solid lines are sigmoidal fits. (b) Zero-field μSR time spectra at 3.5 K. (c) Field distribution for the dynamic spins σ as a function of temperature at 2.27 GPa. (d) Muon asymmetry in different longitudinal fields at the pressure of 2.14 GPa at 2 K.

incommensurate order, a nontrivial function of the asymmetry decay can be expected. However, after trying several functions, we have found that a simple sum of three cosines with the oscillation frequencies of 2.7, 3.3, and 4 MHz reproduces the spectrum quite well [30],

$$A(t) = \frac{2}{3}\sum_{i=1}^{3} A_i \cos(\omega_i t + \phi) e^{-\lambda_T t} + \frac{1}{3} e^{-\lambda_L t}, \qquad (1)$$

where λ_T and λ_L represent, respectively, the transverse and longitudinal relaxation rates, ω is the oscillation frequency, and $\phi \simeq 0$ is the phase. The temperature dependence of the frequencies follows a phenomenological relation $\omega(T) = \omega(0)[1-(T/T_N)^{\alpha'}]^{\beta'}$ with $\alpha' \simeq 4.6$ and $\beta' \simeq 0.5$ (see Supplemental Material [32]). This β' value indicates a mean-field-type magnet, whereas the large α' value supports a complex magnetic state [57].

Experiments performed with a weak transverse field (WTF) of 50 G give access to the model-independent evaluation of the transition temperature and magnetically ordered volume fraction [58]. In the presence of the WTF, static spins do not contribute to the oscillating signal, and the asymmetry directly measures the fraction of dynamic spins in the sample. Figure 3(a) indicates that at ambient pressure this fraction sharply drops down to zero at $T_N \simeq 38$ K. At higher pressures, less than half of the spins become static, whereas the remaining ones are dynamic down to the lowest temperature probed in our experiment.

The crossover temperature, where part of the spins becomes static, was estimated by fitting the temperature dependence of the nonmagnetic volume fraction with a sigmoidal function. We detect a slight increase in T_N at the pressure of 1.19 GPa, in agreement with the magnetization and thermal expansion data. Upon further compression, the crossover temperature decreases to about 15 K. It no longer represents the magnetic ordering temperature, because static spins form a glassy state. This is evidenced by the zero-field data measured at 3.5 K [Fig. 3(b)]. The oscillations due to the long-range-ordered state remain at the same frequencies, but reduce in magnitude upon compression and vanish above 1.37 GPa.

We now turn our attention to the nature of the high-pressure magnetic state. The signal at high pressures is described by a sum of an oscillating function and a Gaussian relaxing function. The total asymmetry includes two contributions, one from the frozen part (A_{fr}) [59] and the other one ($1-A_{\mathrm{fr}}$) that is described by a Gaussian relaxation component $e^{-(\sigma t)^2/2}$, where σ represents the width of the local field distribution. The A_{fr} has been estimated from the WTF measurements. The width of the local magnetic field is estimated to be about 10 G at 4 K. A longitudinal magnetic field, which is 10 times higher than that, should decouple the muon relaxation channel completely. However, even at a longitudinal magnetic field of 500 Oe a weak relaxation survives [Fig. 3(d)], which implies that correlations of unfrozen spins are dynamic in nature. The extracted temperature dependence [Fig. 3(c)] shows an increase in σ below 30 K, indicating the onset of short-range correlations between the dynamic spins, and parallels the formation of frozen spins. Below 15 K, both σ and the fraction of frozen spins remain constant, indicating phase separation of β-Li_2IrO_3 into frozen spins (spin glass) and dynamic spins (spin liquid).

Crystal structure and exchange couplings.—Single-crystal x-ray diffraction (XRD) performed under pressures up to 3.45 GPa does not reveal any drastic structural changes and excludes structural dimerization [29], either macroscopic or local, as the possible cause for the absence

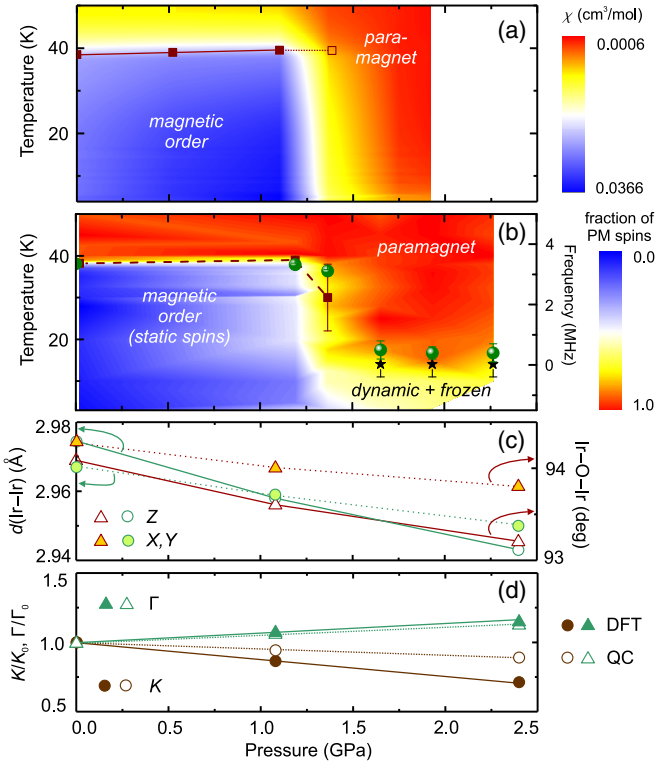

FIG. 4. Phase diagram of β-Li_2IrO_3 as a function of pressure according to (a) susceptibility measurements and (b) μSR data. The circles, squares, and stars correspond, respectively, to the oscillation frequency, T_N, and to the temperature below which the phase-separated state occurs. (c) Changes in the nearest-neighbor Ir-Ir distances and Ir-O-Ir angles under pressure for the X, Y- and Z-type bonds [32]. (d) Relative changes in the Kitaev exchange K and off-diagonal anisotropy Γ with respect to their ambient-pressure values K_0 and Γ_0, respectively. The K and Γ values are averaged over the X, Y and Z bonds. The open and field symbols are from quantum-chemical (QC) and DFT calculations, respectively.

of magnetic order above 1.37 GPa. The orthorhombic symmetry of β-Li_2IrO_3 is preserved, and the Ir displacement parameters remain unchanged under pressure [32]. The Ir-Ir distances were extracted directly from the XRD data, whereas oxygen positions were additionally refined *ab initio* [32], resulting in a smooth pressure dependence. Not only the Ir-Ir distances are shortened, but also Ir-O-Ir angles are reduced by nearly 1° upon the compression to 2.4 GPa [Fig. 4(c)].

The effect of this structural evolution was examined by electronic-structure calculations employing two complementary approaches: (i) second-order perturbation theory for an effective model parametrized from density-functional (DFT) calculations [60], and (ii) multireference quantum chemistry calculations for finite embedded clusters [61]. Both methods agree on the qualitative trends for nearest-neighbor exchange couplings, namely, the absolute values of the off-diagonal exchange interaction Γ increases, whereas the Kitaev exchange K decreases [Fig. 4(d)]. The Heisenberg J, as well as all couplings beyond nearest neighbors, remain weaker than the nearest-neighbor Γ and K [32].

Discussion.—β-Li_2IrO_3 reveals dissimilar trends upon compression. The increasing T_N indicates growing energies of exchange couplings, as the Ir-Ir distances shorten. In contrast, the reduction in H_c points to a destabilization of the ambient-pressure magnetic order. Recent theory work [21] considers β-Li_2IrO_3 from the perspective of two competing ordering modes. The ambient-pressure incommensurate order is due to a $Q \neq 0$ mode, which is predominant in zero field. A magnetic field applied along the b direction amplifies the $Q = 0$ mode and reduces the magnitude of the $Q \neq 0$ mode, eventually destroying incommensurate order above H_c. Our data evidence the stabilization of the $Q = 0$ mode and destabilization of the $Q \neq 0$ mode also under pressure, which is concomitant with the reduction in K and the increase in Γ, as our *ab initio* results show [Fig. 4(d)]. Around 1.4 GPa, the $Q \neq 0$ mode is no longer active, and the incommensurate order disappears.

Two scenarios of this breakdown can be envisaged. According to Ref. [21], the $\Gamma/K > 1$ region should be characterized by another type of magnetic order, which may appear in the narrow pressure range around 1.4 GPa before the spin-liquid phase of the large-Γ limit [24] sets in. However, our data are also consistent with a direct first-order transformation between the incommensurate order and spin liquid, similar to the pressure-induced breakdown of magnetic order in itinerant magnets, where phase separation is typically observed, with ordered and disordered phases coexisting in a broad pressure range [62]. Indeed, at low temperatures, we observe a fraction of disordered spins already at 1.19 GPa, as well as the coexistence of ordered and disordered states at 1.36 GPa, thus confirming the first-order nature of the transition [Fig. 3(a)]. The reduced magnetization at 1.37 GPa (Fig. 1) would be then due to the coexistence of the ordered phase and spin liquid.

Interestingly, the ground state of β-Li_2IrO_3 well above 1.4 GPa is also phase separated, but this time it represents a mixture of two disordered states: spin liquid and spin glass. Similar features have been seen in powder samples of the kagome mineral vesigneite [63], although single crystals of the same mineral show clear signatures of a magnetic transition [64], thus hinting at the structural disorder as the origin of both the dynamic spin state and partial freezing therein.

β-Li_2IrO_3 is clearly different, because it does show robust magnetic order at ambient pressure and, according to XRD data [32], lacks any visible structural defects, either native or pressure induced. Therefore, we are led to conclude that dynamic spins in pressurized β-Li_2IrO_3 represent a spin-liquid state, but this liquid is highly fragile. A strong tendency toward freezing is more likely to occur

in a classical spin liquid, which is indeed anticipated in the large-Γ limit that our system approaches. With $\Gamma < 0$, exchange terms beyond Γ should cause order by disorder, but its energy scale is as low as $\Gamma/64 \leq 3$ K, going beyond the lower limit of our data.

Conclusions.—Incommensurate magnetic order in β-Li_2IrO_3 is destabilized under pressure and vanishes upon the first-order transition around 1.4 GPa, giving way to the coexisting dynamic and static spins in a partially frozen spin liquid. A plausible explanation of this effect is the formation of a classical spin liquid prone to spin freezing. Such a state is indeed expected in the large-Γ limit that β-Li_2IrO_3 tends to approach. Our results do not support the pressure-induced formation of a quantum spin liquid, and instead put pressurized β-Li_2IrO_3 forward as a suitable platform for studying classical spin liquid in the large-Γ limit of the extended Kitaev model, an interesting and hitherto unexplored field. The natural next step in this endeavor would be nuclear magnetic resonance and electron spin resonance measurements probing spin dynamics in pressurized β-Li_2IrO_3 on different timescales.

A. A. T. is indebted to Ioannis Rousochatzakis for insightful conversations and sharing his unpublished results. We also acknowledge fruitful discussions with Steve Winter and Radu Coldea and the provision of the μSR beam time by PSI and ISIS. R. S. M. would like to thank Dr. Naoyuki Tateiwa and Dr. Yoshifumi Tokiwa for their suggestions on optimizing parameters of the pressure cell. The work in Augsburg was supported by DFG under TRR80 (F. F., A. A. T., P. G.) and JE-748/1 (A. J. E), and by the Federal Ministry for Education and Research through the Sofja Kovalevskaya Award of Alexander von Humboldt Foundation (M. M., T. D., A. A. T.). The work of G. S. is supported by the Swiss National Science Foundation Grants No. 200021_149486 and No. 200021_175935.

*These authors contributed equally to this work.
†altsirlin@gmail.com

[1] L. Savary and L. Balents, Quantum spin liquids: A review, Rep. Prog. Phys. **80**, 016502 (2017).
[2] A. Kitaev, Anyons in an exactly solved model and beyond, Ann. Phys. (Amsterdam) **321**, 2 (2006).
[3] S. Trebst, Kitaev materials, arXiv:1701.07056.
[4] S. M. Winter, A. A. Tsirlin, M. Daghofer, J. van den Brink, Y. Singh, P. Gegenwart, and R. Valentí, Models and materials for generalized Kitaev magnetism, J. Phys. Condens. Matter **29**, 493002 (2017), and references therein.
[5] M. Hermanns, I. Kimchi, and J. Knolle, Physics of the Kitaev model: Fractionalization, dynamic correlations, and material connections, Annu. Rev. Condens. Matter Phys. **9**, 17 (2018).
[6] J. Knolle, D. L. Kovrizhin, J. T. Chalker, and R. Moessner, Dynamics of a Two-Dimensional Quantum Spin Liquid: Signatures of Emergent Majorana Fermions and Fluxes, Phys. Rev. Lett. **112**, 207203 (2014).
[7] J. Nasu, J. Knolle, D. L. Kovrizhin, Y. Motome, and R. Moessner, Fermionic response from fractionalization in an insulating two-dimensional magnet, Nat. Phys. **12**, 912 (2016).
[8] S. Mandal and N. Surendran, Exactly solvable Kitaev model in three dimensions, Phys. Rev. B **79**, 024426 (2009).
[9] A. Smith, J. Knolle, D. L. Kovrizhin, J. T. Chalker, and R. Moessner, Neutron scattering signatures of the 3D hyperhoneycomb Kitaev quantum spin liquid, Phys. Rev. B **92**, 180408(R) (2015).
[10] B. Perreault, J. Knolle, N. B. Perkins, and F. J. Burnell, Theory of Raman response in three-dimensional Kitaev spin liquids: Application to β- and γ-Li_2IrO_3 compounds, Phys. Rev. B **92**, 094439 (2015).
[11] J. Nasu, T. Kaji, K. Matsuura, M. Udagawa, and Y. Motome, Finite-temperature phase transition to a quantum spin liquid in a three-dimensional Kitaev model on a hyperhoneycomb lattice, Phys. Rev. B **89**, 115125 (2014).
[12] I. Kimchi, J. G. Analytis, and A. Vishwanath, Three-dimensional quantum spin liquids in models of harmonic-honeycomb iridates and phase diagram in an infinite-D approximation, Phys. Rev. B **90**, 205126 (2014).
[13] J. Nasu, M. Udagawa, and Y. Motome, Vaporization of Kitaev Spin Liquids, Phys. Rev. Lett. **113**, 197205 (2014).
[14] A. Biffin, R. D. Johnson, S. Choi, F. Freund, S. Manni, A. Bombardi, P. Manuel, P. Gegenwart, and R. Coldea, Unconventional magnetic order on the hyperhoneycomb Kitaev lattice in β-Li_2IrO_3: Full solution via magnetic resonant x-ray diffraction, Phys. Rev. B **90**, 205116 (2014).
[15] T. Takayama, A. Kato, R. Dinnebier, J. Nuss, H. Kono, L. S. I. Veiga, G. Fabbris, D. Haskel, and H. Takagi, Hyperhoneycomb Iridate β-Li_2IrO_3 as a Platform for Kitaev Magnetism, Phys. Rev. Lett. **114**, 077202 (2015).
[16] A. Biffin, R. D. Johnson, I. Kimchi, R. Morris, A. Bombardi, J. G. Analytis, A. Vishwanath, and R. Coldea, Noncoplanar and Counterrotating Incommensurate Magnetic Order Stabilized by Kitaev Interactions in γ-Li_2IrO_3, Phys. Rev. Lett. **113**, 197201 (2014).
[17] K. A. Modic, T. E. Smidt, I. Kimchi, N. P. Breznay, A. Biffin, S. Choi, R. D. Johnson, R. Coldea, P. Watkins-Curry, G. T. McCandless, J. Y. Chan, F. Gandara, Z. Islam, A. Vishwanath, A. Shekhter, R. D. McDonald, and J. G. Analytis, Realization of a three-dimensional spin-anisotropic harmonic honeycomb iridate, Nat. Commun. **5**, 4203 (2014).
[18] I. Kimchi, R. Coldea, and A. Vishwanath, Unified theory of spiral magnetism in the harmonic-honeycomb iridates α, β, and γ-Li_2IrO_3, Phys. Rev. B **91**, 245134 (2015).
[19] E. K.-H. Lee and Y. B. Kim, Theory of magnetic phase diagrams in hyperhoneycomb and harmonic-honeycomb iridates, Phys. Rev. B **91**, 064407 (2015).
[20] E. K.-H. Lee, J. G. Rau, and Y. B. Kim, Two iridates, two models, and two approaches: A comparative study on magnetism in three-dimensional honeycomb materials, Phys. Rev. B **93**, 184420 (2016).
[21] S. Ducatman, I. Rousochatzakis, and N. B. Perkins, Magnetic structure and excitation spectrum of the hyperhoneycomb Kitaev magnet β-Li_2IrO_3, Phys. Rev. B **97**, 125125 (2018).

[22] H.-S. Kim, Y. B. Kim, and H.-Y. Kee, Revealing frustrated local moment model for pressurized hyperhoneycomb iridate: Paving the way toward a quantum spin liquid, Phys. Rev. B **94**, 245127 (2016).

[23] L. S. I. Veiga, M. Etter, K. Glazyrin, F. Sun, C. A. Escanhoela, Jr., G. Fabbris, J. R. L. Mardegan, P. S. Malavi, Y. Deng, P. P. Stavropoulos, H.-Y. Kee, W. G. Yang, M. van Veenendaal, J. S. Schilling, T. Takayama, H. Takagi, and D. Haskel, Pressure tuning of bond-directional exchange interactions and magnetic frustration in the hyperhoneycomb iridate β-Li_2IrO_3, Phys. Rev. B **96**, 140402(R) (2017).

[24] I. Rousochatzakis and N. B. Perkins, Classical Spin Liquid Instability Driven by Off-Diagonal Exchange in Strong Spin-Orbit Magnets, Phys. Rev. Lett. **118**, 147204 (2017).

[25] A. Ruiz, A. Frano, N. P. Breznay, I. Kimchi, T. Helm, I. Oswald, J. Y. Chan, R. J. Birgeneau, Z. Islam, and J. G. Analytis, Correlated states in β-Li_2IrO_3 driven by applied magnetic fields, Nat. Commun. **8**, 961 (2017).

[26] I. Rousochatzakis and N. B. Perkins, Magnetic field-induced evolution of intertwined orders in the Kitaev magnet β-Li_2IrO_3, Phys. Rev. B **97**, 174423 (2018).

[27] W. Knafo, C. Meingast, S. Sakarya, N. H. van Dijk, Y. Huang, H. Rakoto, J.-M. Broto, and H. v. Löhneysen, Critical scaling of the magnetization and magnetostriction in the weak itinerant ferromagnet UIr, J. Phys. Soc. Jpn. **78**, 043707 (2009).

[28] F. Weickert, R. Küchler, A. Steppke, L. Pedrero, M. Nicklas, M. Brando, F. Steglich, M. Jaime, V. S. Zapf, A. Paduan-Filho, K. A. Al-Hassanieh, C. D. Batista, and P. Sengupta, Low-temperature thermodynamic properties near the field-induced quantum critical point in $NiCl_2$-4SC$(NH_2)_2$, Phys. Rev. B **85**, 184408 (2012).

[29] V. Hermann, M. Altmeyer, J. Ebad-Allah, F. Freund, A. Jesche, A. A. Tsirlin, M. Hanfland, P. Gegenwart, I. I. Mazin, D. I. Khomskii, R. Valentí, and C. A. Kuntscher, Competition between spin-orbit coupling, magnetism, and dimerization in the honeycomb iridates: α-Li_2IrO_3 under pressure, Phys. Rev. B **97**, 020104(R) (2018).

[30] A sum of two sites in a helical state, similar to the case of MnGe [31], reproduced the spectrum almost equally well, but introduced unnecessary complications into the analysis.

[31] N. Martin, M. Deutsch, F. Bert, D. Andreica, A. Amato, P. Bonfá, R. De Renzi, U. K. Rößler, P. Bonville, L. N. Fomicheva, A. V. Tsvyashchenko, and I. Mirebeau, Magnetic ground state and spin fluctuations in MnGe chiral magnet as studied by muon spin rotation, Phys. Rev. B **93**, 174405 (2016).

[32] See Supplemental Material at http://link.aps.org/supplemental/10.1103/PhysRevLett.120.237202 for additional experimental details, crystallographic information, and a full list of the computed exchange parameters, which includes Refs. [33–56].

[33] F. Freund, S. C. Williams, R. D. Johnson, R. Coldea, P. Gegenwart, and A. Jesche, Single crystal growth from separated educts and its application to lithium transition-metal oxides, Sci. Rep. **6**, 35362 (2016).

[34] V. Petříček, M. Dušek, and L. Palatinus, Crystallographic computing system JANA2006: General features, Z. Kristallogr. **229**, 345 (2014).

[35] Rigaku Oxford Diffraction, CrysAlisPro Software System Version 1.171.37.35, Rigaku Corp., Oxford, U.K. (2014).

[36] G. M. Sheldrick, SHELXT—Integrated space-group and crystal-structure determination, Acta Crystallogr. Sect. A **71**, 3 (2015).

[37] G. M. Sheldrick, A history of SHELX, Acta Crystallogr. Sect. A **64**, 112 (2008).

[38] N. Tateiwa, Y. Haga, Z. Fisk, and Y. Ŏnuki, Miniature ceramic-anvil high-pressure cell for magnetic measurements in a commercial superconducting quantum interference device magnetometer, Rev. Sci. Instrum. **82**, 053906 (2011).

[39] N. Tateiwa, Y. Haga, T. D. Matsuda, Z. Fisk, S. Ikeda, and H. Kobayashi, Note: Improved sensitivity of magnetic measurements under high pressure in miniature ceramic anvil cell for a commercial SQUID magnetometer, Rev. Sci. Instrum. **84**, 046105 (2013).

[40] More information on MPMS Application Note 1014-213 can be found at http://www.qdusa.com/sitedocs/appNotes/mpms/1014-213.pdf.

[41] T. H. K. Barron, J. G. Collins, and G. K. White, Thermal expansion of solids at low temperatures, Adv. Phys. **29**, 609 (1980).

[42] R. S. Manna, B. Wolf, M. de Souza, and M. Lang, High-resolution thermal expansion measurements under helium-gas pressure, Rev. Sci. Instrum. **83**, 085111 (2012).

[43] R. Küchler, T. Bauer, M. Brando, and F. Steglich, A compact and miniaturized high resolution capacitance dilatometer for measuring thermal expansion and magnetostriction, Rev. Sci. Instrum. **83**, 095102 (2012).

[44] R. Khasanov, Z. Guguchia, A. Maisuradze, D. Andreica, M. Elender, A. Raselli, Z. Shermadini, T. Goko, F. Knecht, E. Morenzoni, and A. Amato, High pressure research using muons at the Paul Scherrer Institute, High Press. Res. **36**, 140 (2016).

[45] G. Kresse and J. Furthmüller, Efficiency of ab-initio total energy calculations for metals and semiconductors using a plane-wave basis set, Comput. Mater. Sci. **6**, 15 (1996).

[46] G. Kresse and J. Furthmüller, Efficient iterative schemes for *ab initio* total-energy calculations using a plane-wave basis set, Phys. Rev. B **54**, 11169 (1996).

[47] J. P. Perdew, A. Ruzsinszky, G. I. Csonka, O. A. Vydrov, G. E. Scuseria, L. A. Constantin, X. Zhou, and K. Burke, Restoring the Density-Gradient Expansion for Exchange in Solids and Surfaces, Phys. Rev. Lett. **100**, 136406 (2008).

[48] K. Koepernik and H. Eschrig, Full-potential nonorthogonal local-orbital minimum-basis band-structure scheme, Phys. Rev. B **59**, 1743 (1999).

[49] J. P. Perdew and Y. Wang, Accurate and simple analytic representation of the electron-gas correlation energy, Phys. Rev. B **45**, 13244 (1992).

[50] H. Eschrig and K. Koepernik, Tight-binding models for the iron-based superconductors, Phys. Rev. B **80**, 104503 (2009).

[51] D. Figgen, K. A. Peterson, M. Dolg, and H. Stoll, Energy-consistent relativistic pseudopotentials and correlation consistent basis sets for the 5d elements Hf-Pt, J. Chem. Phys. **130**, 164108 (2009).

[52] T. H. Dunning, Gaussian basis sets for use in correlated molecular calculations. I. The atoms boron through neon and hydrogen, J. Chem. Phys. **90**, 1007 (1989).

[53] K. Pierloot, B. Dumez, P.-O. Widmark, and B. O. Roos, Density matrix averaged atomic natural orbital ANO basis sets for correlated molecular wave functions, Theor. Chim. Acta **90**, 87 (1995).

[54] H. J. Werner, P. J. Knowles, G. Knizia, F. R. Manby, and M. Schütz, Molpro: A general-purpose quantum chemistry program package, Comput. Mol. Sci. **2**, 242 (2012).

[55] R. Yadav, N. A. Bogdanov, V. M. Katukuri, S. Nishimoto, J. van den Brink, and L. Hozoi, Kitaev exchange and field-induced quantum spin-liquid states in honeycomb α-$RuCl_3$, Sci. Rep. **6**, 37925 (2016).

[56] S. Nishimoto, V. M. Katukuri, V. Yushankhai, H. Stoll, U. K. Rößler, L. Hozoi, I. Rousochatzakis, and J. van den Brink, Strongly frustrated triangular spin lattice emerging from triplet dimer formation in honeycomb Li_2IrO_3, Nat. Commun. **7**, 10273 (2016).

[57] M. Smidman, D. T. Adroja, A. D. Hillier, L. C. Chapon, J. W. Taylor, V. K. Anand, R. P. Singh, M. R. Lees, E. A. Goremychkin, M. M. Koza, V. V. Krishnamurthy, D. M. Paul, and G. Balakrishnan, Neutron scattering and muon spin relaxation measurements of the noncentrosymmetric antiferromagnet $CeCoGe_3$, Phys. Rev. B **88**, 134416 (2013).

[58] While the main results obtained using the WTF are quite robust, the determination of the volume fraction needs to be taken with caution if static fields in the sample are on the order of the applied field. Hence, the ordered fraction in the figure (color plot) in the high-pressure phase is only indicative but not absolute. It is to be noted that the background contribution has been subtracted to get 100% magnetic volume fraction at ambient pressure.

[59] We used an oscillatory function for the frozen spins and arrived at zero oscillation frequency, which corresponds to the absence of static fields typical for a glassy state, as opposed to the nonzero frequencies characteristic of the long-range-ordered state below 1.37 GPa.

[60] S. M. Winter, Y. Li, H. O. Jeschke, and R. Valentí, Challenges in design of Kitaev materials: Magnetic interactions from competing energy scales, Phys. Rev. B **93**, 214431 (2016).

[61] V. M. Katukuri, R. Yadav, L. Hozoi, S. Nishimoto, and J. van den Brink, The vicinity of hyper-honeycomb β-Li_2IrO_3 to a three-dimensional Kitaev spin liquid state, Sci. Rep. **6**, 29585 (2016).

[62] Y. J. Uemura *et al.*, Phase separation and suppression of critical dynamics at quantum phase transitions of MnSi and $(Sr_{1-x}Ca_x)RuO_3$, Nat. Phys. **3**, 29 (2007), and references therein.

[63] R. H. Colman, F. Bert, D. Boldrin, A. D. Hillier, P. Manuel, P. Mendels, and A. S. Wills, Spin dynamics in the $S = \frac{1}{2}$ quantum kagome compound vesignieite, $Cu_3Ba(VO_5H)_2$, Phys. Rev. B **83**, 180416(R) (2011).

[64] H. Ishikawa, T. Yajima, A. Miyake, M. Tokunaga, A. Matsuo, K. Kindo, and Z. Hiroi, Topochemical crystal transformation from a distorted to a nearly perfect kagome cuprate, Chem. Mater. **29**, 6719 (2017).